International Journal of Thermofluid Science and Technology (2022)
Volume 9, Issue 3, Paper No. 090301
https://doi.org/10.36963/IJTST.2022090301
Research Article

CFD Investigation of flow reversal in inverted U-tube steam generator under two-phase natural circulation

Waqar Riaz*, Ammar Ahmed, Kamran Rasheed Qureshi

Pakistan Institute of Engineering and Applied Sciences (PIEAS), Nilore, Islamabad, Pakistan

ARTICLE INFO

Received: 15 Nov. 2021;
Received in revised form:
01 Jan. 2022;
Accepted: 25 Jan. 2022;
Published online:
12 Feb. 2022

Keywords:
Two-phase NC
U-tube steam generator
Operating flow rate
CFD
Natural circulation

ABSTRACT

In this paper, a critical mass flow rate (CMFR) has been obtained for three different steam generators (i.e. two marine-type and one commercial) at different inlet void fractions using the CFD method to study the sustainability of natural circulation (NC) due to depressurization in two-phase NC mode. Because of depressurization, the transients in the inlet void fraction have been considered as multiple steady-state inputs, and the range of safe operating mass flow rate has been obtained. The results show that the characteristics curves shift with inlet void fraction thus limiting the operating mass flow rate range between 0.046 kg/s to 0.050 kg/s for M_SG1 and 0.051 kg/s to 0.055 kg/s for M_SG2. The effect of pipe roughness on CMFR has also been studied. The results can be used for the optimized design of the U-tube steam generator (UTSG) that will safely perform the heat removal operation during a small break loss of coolant accident (SBLOCA).

1. Introduction

An important passive phenomenon for the inherent safety of nuclear power plant (NPP) is NC that eliminates the need for external power sources and human intervention [1]. The systems utilizing this phenomenon are characterized by a small driving force as compared to the systems which are externally driven. NC-based systems are highly sensitive to pipe losses, bend losses, and geometry of the system [2]. The physical phenomenon resulting in NC is quite complex. Several quantitative methods were developed based on different studies for simulating the thermal-hydraulic behavior in NC mode during SBOLCA and showed the importance of steam generator (SG) in removing the core decay heat [3].

The most effective modes of heat transfer from the primary side to the secondary side of SG are single and two phase-NC, and reflux condensation in case of events like the loss of external power, decrease of pressure in the primary loop, stoppage of main pumps, and reduced coolant inventory [4]. LOBI [5], LSTF [6], PACTEL [4], PKL [7], IIST [8] and BETHSY [9] observed and investigated experimentally the thermal-hydraulic behavior of U-tubes in SG and showed the occurrence of these three heat transfer modes and reverse flow in some U-tubes of SG. Reverse flow in U-tubes greatly decreased the heat transfer characteristics from the primary to the

*Corresponding e-mail: waqarriaz@pieas.edu.pk (Waqar Riaz)

secondary side of SG and endangered the NPP's operation.

Nomenclature

CMFR	Critical Mass Flow Rate	SG	Steam Generator
CFD	Computational Fluid Dynamics	M_SG1	Marine Type Steam Generator 1
NC	Natural Circulation	M_SG2	Marine Type Steam Generator 2
NPP	Nuclear Power Plant	C_SG	Commercial Steam Generator
UTSG	U-Tube Steam Generator	SBLOCA	Small Break Loss of Coolant Accident

Sanders [10] obtained the unstable solutions for all U-tubes in SG using single-phase NC theoretical model. Hao, *et al.* [11] experimentally determined the relationship between the U-tube length and the CMFR. For the small length U-tube SG the reverse flow occurred in shorter tubes whereas, for the large length U-tube SG, it occurred in the longer tubes. The factors that affect the reverse flow are the U-tube length and the inlet subcooling which were discussed using the CFD method [12]. They also found a linear relation between critical inlet points and the mass flow rate [13]. Yang, *et al.* [14] extended the research to study the inlet temperature effect on flow instability in small marine-type and commercial SGs. Jeong, *et al.* [15] obtained a judgment criterion for the two-phase reverse flow with a detailed physical explanation of the process and developed a theoretical model for studying two-phase NC. They found that different lengths of U-tube SG have different flow rates and distribution was highly non-uniform. Furthermore, Hu, *et al.* [16] used RELAP5/MOD3.3 for studying transient behavior in single-phase NC. The mass flow rate in U-tube with the reverse flow is found to be greater than the one with the normal flow with reduced heat transfer efficiency in reverse flow. Shen, *et al.* [17] studied the effects of abnormal water levels in the secondary side of UTSG on reverse flow characteristics using 1D single phase model based on perturbation theory and found that the space distribution in smaller SG is insensitive to the water level in the secondary side.

Chu, *et al.* [18] developed a theoretical model to find a two-phase pressure drop in natural circulation. The effects of different U-tube lengths, inlet steam quality, bending radius, and primary side pressure were also analyzed. Chu, *et al.* [19] performed CFD of two-phase NC for saturated secondary side conditions and studied the reverse flow characteristics and its influence factors. The results showed a negative slope region in the characteristics curve. But their study did not predict the operating range of mass flow rates and neglected the flow developing length at the U-tube inlet.

Most of the previous research was focused on just determining the CMFR and void fraction distribution of two-phase NC in U-tube SG. The two most important parameters that were neither determined nor discussed in previous studies are the safe operating mass flow rate range for SG to work effectively in two-phase NC mode in case of transients in inlet void fraction and the pipe roughness effect on two-phase NC in SG. In this paper, one commercial SG and two marine-type SGs have been simulated in ANSYS Fluent to determine the safe operating mass flow rate range under transient inlet void fraction. The transients have been considered as multiple point steady-state processes by analyzing the U-tube at different inlet void fractions for the whole range of mass flow rates. The safe and sustainable operating range for mass flow rate has been selected based on limits set by the characteristics curves at different inlet void fractions. The SG can be operated safely within the flow rate range. The effect of pipe roughness on the characteristics curve and hence the CMFR has also been studied. Also, Chu, *et al.* [19] neglected the entrance effect for the primary side of SG, which needs to be included as the fluid enters from the plenum into the U-tube. These entrance effects have been included in the current study, as they affect the void fraction distribution. The results and conclusions of this study are of great significance for the design of NC-based steam generators as well as safe operations of PWRs.

2. Mathematical Model

Consider an inverted U-tube of height H, bending radius R, and tube diameter d of the

steam generator as shown in Fig 1. A 1-dimensional coordinate system is attached along the length of the U-tube in which the distance 's' represents the position from the U-tube inlet. The two-phase mixture from the reactor pressure vessel enters from point 'a' of U-tube at inlet temperature T_a. It then moves through the inverted U-tube and exits from point 'b' at outlet temperature T_b thereby transferring the heat to the secondary side of the U-tube. The net pressure gradient [18] between the inlet and outlet of the U-tube can be written as

$$\frac{dp}{ds} = \left(\frac{dp_{tp}}{ds}\right)_f + \left(\frac{dp_{sp}}{ds}\right)_f + \left(\frac{dp}{ds}\right)_b \quad (1)$$

Whereas

$\left(\frac{dp_{tp}}{ds}\right)_f$ is the two-phase frictional pressure gradient

$\left(\frac{dp_{sp}}{ds}\right)_f$ is the single-phase frictional pressure gradient

$\left(\frac{dp}{ds}\right)_b$ is the bending pressure gradient

And $\left(\frac{dp_g}{ds}\right)$ is the gravitational pressure gradient

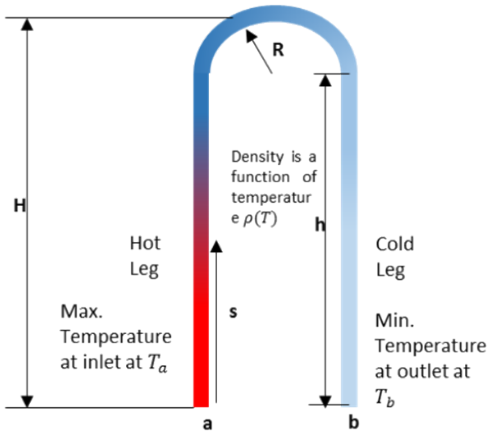

Fig. 1. Inverted U-tube of steam generator

The net pressure drop can be calculated by solving the Eq. **Error! Reference source not found.**. If the net pressure drop at a particular flow rate is negative between the inlet and outlet of the U-tube, then the flow will be density-driven (natural flow). A characteristics curve can be obtained by solving the pressure gradient equation at different mass flow rates. Because of the two-phase flow, the solution to the pressure gradient equation at saturated secondary side conditions for U-tube SG requires empirical correlations. A CFD methodology is selected to obtain the characteristics curves.

3. CFD Methodology

3.1 Geometry

Typical inverted U-tube steam generators were selected, which are widely used in PWRs. To investigate the natural circulation behavior in two-phase flow during SBLOCA, working conditions and U-tube dimensions were taken from two marine-type NPP SGs [19] and one commercial SG. The details of the dimensions for all SGs are shown in Fig 2.The FLUENT model for the SG U-tube is shown in Fig 3. "V1" represents the vertical straight length and "R3" represents the bending radius calculated based on bending length.

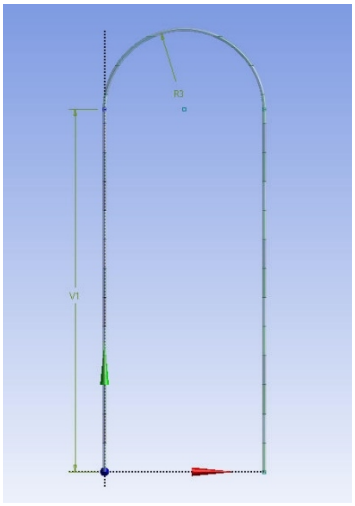

Fig. 2. Geometry of Inverted U-tube

3.2 Mesh Independence

Meshing independence was performed for the structured mesh generated in U-tube. Fig 3 shows a discrepancy in the critical flow rates at different meshing.

The flow rate approaches a single value with a relative error of less than 0.1%. So, the critical flow rate is almost independent of the meshing details. Fig 4 shows the characteristics curve obtained at different meshing which also shows independence on mesh elements. The selected mesh as shown in Fig 5 had quality greater than 85% with minimum pressure and CMFR

variation.

Table. 1 Dimensions of SGs

	M_SG1	M_SG2	C_SG
Straight Length (m)	1.25	2.5	7
Bending Length (m)	0.865	1.73	4.3
Tube Diameter (m)	0.013	0.013	0.0194

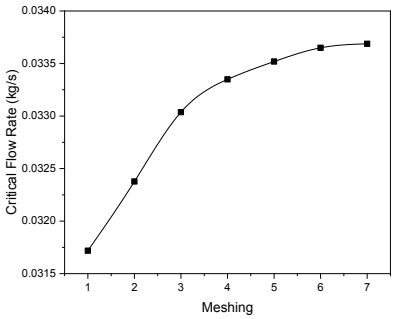

Fig. 3. Critical mass flow rate with meshing

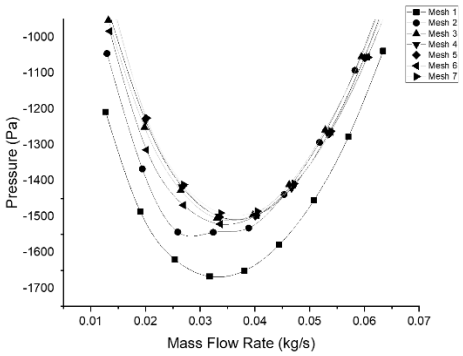

Fig. 4. Characteristics curves at different meshing

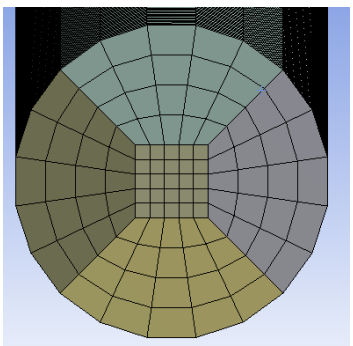

Fig. 5. Inlet cross-section of U-tube

3.3 Boundary Conditions

Velocity inlet is specified at the inlet whereas pressure is specified at the outlet as boundary conditions. Water-liquid and water-vapors with variable fluid properties were used as a two-phase mixture. Variation of fluid properties was incorporated using eighteen interpolation points as a function of local temperature and pressure for density, specific heat, viscosity, and thermal conductivity for both water-liquid and water-vapors.

Saturated temperatures were selected at the U-tube inlet for liquid and vapors. The U-tube wall temperature T_w was considered as constant value at saturated secondary side conditions (Jeong, *et al.* [15]). The mass flow rate was increased slowly by a stepwise increase in the velocities of both phases. The detailed flow conditions for all SGs are given in Fig 6.

Table. 2 Flow Conditions for SGs

	M_SG1& M_SG2	**C_SG**
Primary Side Pressure (MPa)	9	15.2
Wall Temperature (K)	490	543
Fluid Inlet Temperature (K)	573	616
Inlet Liquid Velocity (m/s)	0.1-1.4	0.1-2.4
Inlet Void Fraction	0.1-0.4	0.1-0.4
Pipe Roughness(μm)	Smooth to 250 & Nil	Smooth

3.4 Solver Settings

A pressure-based solver coupled with absolute velocity formulation was selected in FLUENT simulation general settings. Gravity in a vertical direction (i.e along the y-axis) was also specified to study the effect of change in density. The "Phase Coupled SIMPLE" scheme and standard initialization method was chosen. A convergence criterion of 0.0001 was used for the solution.

4. Multiphase Models

Eulerian Model was chosen provided in ANSYS Fluent because the void fraction was greater than 10%, which continuously changed along the U-tube hot leg. It was the most suitable one from the available models to simulate the condensing vapors in the case of

natural circulation.

The standard k-ε model with dispersed turbulence was chosen with standard wall functions because of reasonable accuracy and wide industrial applications. The general conservation equations solved by the Eulerian model are given below:

The continuity equation for the q_{th} phase is:

$$\frac{\partial}{\partial t}(\alpha_q \rho_q) + \nabla.(\alpha_q \rho_q \vec{v}_q) = \sum_{p=1}^{n} (\dot{m}_{pq} - \dot{m} \quad (2)$$

Whereas t is time, α_q is the void fraction, ρ_q is density and $\vec{v}_q$is velocity. The mass transfer from one to the other is represented by $\dot{m}_{pq}$ (from p to q) and $\dot{m}_{qp}$ (from q to p). S_q is the mass source term and n is the total number of other phases.

The momentum equation for the q_{th} phase is:

$$\frac{\partial}{\partial t}(\alpha_q \rho_q \vec{v}_q) + \nabla.(\alpha_q \rho_q \vec{v}_q \vec{v}_q) = -\alpha_q \nabla p \quad (3)$$
$$+ \left(\vec{F}_q + \vec{F}_{lift,q} + \vec{F}_{wl,q} + \right.$$

where p is the static pressure, $\overline{\overline{\tau}_q}$is the stress-strain tensor, $\vec{g}$ is gravitational force and $\vec{R}_{pq}$ is the interaction force between two different phases. $\vec{F}_{lift,q}$, $\vec{F}_{wl,q}$, $\vec{F}_{td,q}$, $\vec{F}_q$, $\vec{F}_{vm,q}$ are lift force, wall-lubrication force, turbulent dispersion force, the external body force, and virtual-mass force respectively.

The energy equation for the q_{th} phase is:

$$\frac{\partial}{\partial t}(\alpha_q \rho_q h_q) + \nabla.(\alpha_q \rho_q \vec{u}_q h_q) = \alpha_q \frac{\partial p_q}{\partial t} \cdot \quad (4)$$

Whereas h_q is qth phase enthalpy, $\vec{q}_q$ is the heat flux, $S_q$is the source term for energy, Q_{pq} is the amount of heat exchange between two phases and h_{pq} is the interphase enthalpy.

4.1 Interphase Forces

$\vec{R}_{pq}$in Eq (2) represents the interphase interaction force between the phases which can be simplified as [20].

$$\sum_{p=1}^{n} \vec{R}_{pq} = \sum_{p=1}^{n} K_{pq}(\vec{v}_p - \vec{v}_q) \quad (5)$$

Where K_{pq}, the interphase momentum exchange coefficient between the water and vapor phases can be estimated using Schiller and Naumann Model [20], which is expressed as follows:

$$K_{pq} = \frac{\rho_p f}{6\tau_p} d_p A_i \quad (6)$$

Where d_p is the bubble diameter, ρ_p is the density of phase p, τ_p is particulate relaxation time and is given in Eq. (7)

$$\tau_p = \frac{\rho_p d_p^2}{18\mu_q} \quad (7)$$

A_i is the interfacial area which was calculated using the symmetric model and is given by:

$$A_i = \frac{6\alpha_p(1-\alpha_p)}{d_p} \quad (8)$$

f is the drag function which is calculated as:

$$f = \frac{C_D Re}{24} \quad (9)$$

Where Re and C_D represents Reynolds number and drag coefficient respectively.

$$C_D = \begin{cases} 24\frac{(1+0.15Re^{0.687})}{Re} & Re \le 1000 \\ 0.44 & Re > 1000 \end{cases} \quad (10)$$

K_{pq} was calculated using Brucato modification correlation because Schiller and Naumann Model is used for interaction between solid particles and liquid, whereas Brucato modification enables its use for liquid-vapor interaction.

Antal and Lopez de Bertodano models were used for the calculation of wall lubrication and turbulent dispersion respectively in Eq. (2). The dispersed phase i.e water-vapor influences turbulence which was included using the Simonin Model [20].

The effects of the lift force and virtual mass force were very small. Drag force was much larger as compared to the lift force, and the accelerations between the phases were approximately zero. So both of these effects were neglected from Eq. (2), [19].

4.2 Heat and Mass Transfer Models

The volumetric heat transfer rate for vapor and liquid phase can be given as [20]

$$Q_{pq} = h_{pq} A_i (T_p - T_q) \quad (11)$$

Whereas $A_i$is the interfacial area, $(T_p - T_q)$ represents the temperature difference of the two phases and h_{pq} represent the heat transfer coefficient. Ranz Marshall model [20] given in Eq. 11 was used for the calculation of the heat

transfer coefficient.

$$Nu_q = 2.0 + 0.6\mathrm{Re}_{ql}^{1/2}\,\mathrm{Pr}^{1/3} \quad (12)$$

$$h_{qp} = \frac{Nu_q \lambda_l}{d_g} \quad (13)$$

Where Pr is the liquid phase Prandtl number and λ_l is liquid thermal conductivity.

Because of condensation in the hot leg, Lee Model [20] was used for modeling condensation. The model is given as

If $T_l > T_{sat}$ then

$$\dot{m}_{lv} = \text{coeff} * \alpha_l \rho_l \frac{(T_l - T_{sat})}{T_{sat}} \quad (14)$$

If $T_{sat} < T_l$ then

$$\dot{m}_{vl} = \text{coeff} * \alpha_v \rho_v \frac{(T_{sat} - T_v)}{T_{sat}} \quad (15)$$

This model requires the fine-tuning of "coeff" with the experimental data. Its value can vary from 0.1 to several thousand depending on experimental conditions [21].

5. Model Validation

For validation of the multiphase model, nine data points were taken from the natural circulation experiment performed by Jain [22] in the vertical test section of length 2.44 m and diameter 20.6 mm as shown in Table 3. Subcooled water entered the test section and was uniformly heated to boil. The constant wall temperature boundary condition was replaced with constant heat flux to meet the experimental need. Chu, *et al.* [19] showed that replacing the boundary condition will not affect the modeling method, and if validated, the selected models can be used for both boiling and condensation in small circular diameter tubes.

Table 3

Jain experiment flow conditions

N (Data Point)	Pressure (Mpa)	Heat Flux (kW/m^2)	Inlet Velocity (m/s)	Sub-cooling (K)
1	1.38	64.64	1.676	2
2	4.14	222.43	1.768	2
3	4.14	152.72	1.524	9
4	6.9	283.26	1.524	19
5	6.9	342.19	1.768	8
6	9.65	451.2	1.768	10
7	9.65	162.23	1.402	10
8	10.34	378.31	1.676	1
9	10.34	480.97	1.676	2

A CFD study was performed using the above-mentioned models for calculation of two-phase pressure drop in a vertical tube. Fig 6 shows a comparison of the pressure drop obtained from CFD and Jain [22] experiments. The results were closely related and lie within an error of 15%. The models used in this study were suitable for the calculation of pressure drops in small circular diameter pipes in two-phase NC flow.

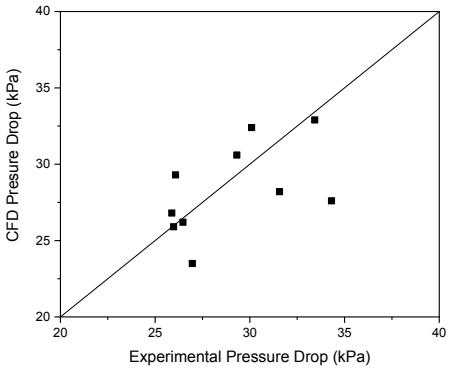

Fig 6. Comparison of CFD and Jain's experiment data

6. Result and Discussion

The inlet mass flow rate is increased by a step-wise increase in inlet velocities of the liquid and vapor phase. The effect of inlet void fraction on CMFR and safe operating flow rate range is determined using the characteristics curves at different inlet void fractions for all SGs. The effect of pipe roughness on the stability of two-phase NC and the entrance effects on void fraction distribution was also found.

6.1 Effect of Pipe Roughness on Two-Phase NC

The characteristics curves for M_SG1 obtained at different pipe roughness are shown in Fig 7. All the curves had a positive sloped region which is stable and a negative slope region, which is unstable [23]. The flow at the point of inflection is called CMFR which is a criterion to check the reverse flow. The pressure drop is the sum of frictional pressure drop and

gravitational pressure drop. The gravitational pressure drop remains the same for constant flow conditions and is independent of pipe roughness. But the frictional pressure drop is a strong function of pipe roughness and increases with an increase in pipe roughness. At higher values of pipe roughness, the frictional pressure drop increases more rapidly as the mass flow rate is increased, which results in the start of a stable region at smaller values of mass flow rate. Fig 8 shows the CMFR variation with pipe roughness. It decreases with an increase in pipe roughness because of increased frictional pressure drop. So the reverse flow is least likely to occur at high pipe roughness but this also limits the maximum NC-based mass flow rate to relatively small values. The net effect is the contraction in the stable as well as the unstable region as pipe roughness increases. Therefore, a balance is required between a pipe roughness and maximum NC mass flow rate for a perfect SG design.

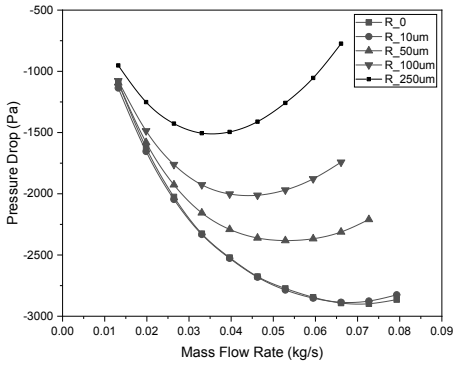

Fig 7. Characteristics curve at different pipe roughness for M_SG1

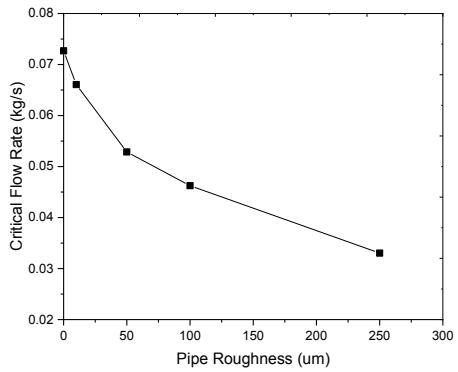

Fig 8. Variation of CMFR with pipe roughness for M_SG1

6.2 Safe Operating Flow Rate Range and Inlet Void Fraction

The characteristics curves for M_SG1, M_SG2, and C_SG at different inlet void fractions are shown in in Fig 9, Fig 10, and Fig 11 respectively. All the curves had a negative slope region showing instability and reverse flow. For M_SG1, the curves were produced for rough pipes whereas for M_SG2 and C_SG smooth pipes were used. The inlet void fraction greatly influences the characteristics curve. The pressure drop in the unstable region increases with an increase in inlet void fraction for all SGs, whereas in the stable region it increases for small void fractions. The characteristics curves at high inlet void fraction in the case of C_SG have more than one critical point because of competition between gravitational and frictional pressure drops. These curves were used to determine the safe operating mass flow rate range if the transients in the inlet void fraction lie in the range. The safe operating flow rate range was obtained using the following strategy:

1. The maximum safe operating flow rate was dictated by the point of transition from natural to forced circulation at a minimum void fraction. The point was obtained by the intersection of the curve at 0.1 void fraction with the horizontal axis. For M_SG1 and M_SG2, these points lie at 0.050 kg/s and 0.0548 kg/s respectively.
2. The minimum operating mass flow rate was dictated by the absolute maximum CMFR at any inlet void fraction from the given operational range and was equal to 0.046 kg/s and 0.518 kg/s for M_SG1 and M_SG2 respectively. The flow will be stable within these ranges with a transient in inlet void fraction.

Fig 11 shows that no such range exists for C_SG with the current range of inlet void fraction. But if the void fraction was controlled and kept below 0.3 then the safe operating mass flow rate range exist which lies between 0.105 kg/s and 0.114 kg/s.

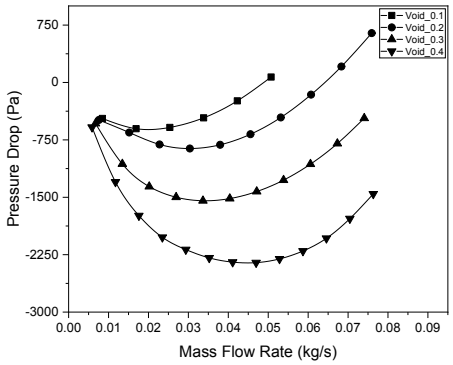

Fig 9. Characteristics curves at different inlet void fraction for M_SG1

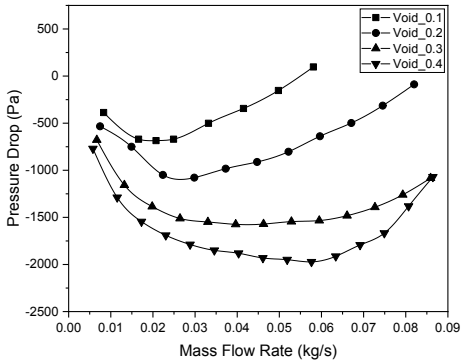

Fig 10. Characteristics curves at different inlet void fraction for M_SG2

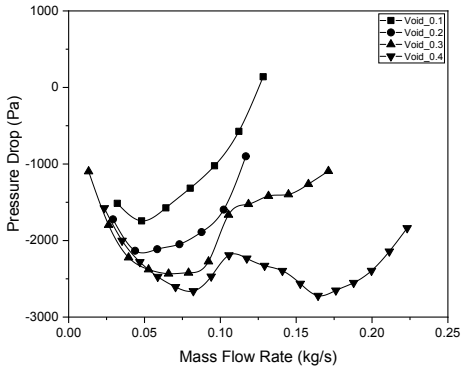

Fig 11. Characteristics curves at different inlet void fraction for M_SG3

6.3 Effect of Inlet Void Fraction on CMFR

Fig 12 and Fig 13 show that the CMFR increases linearly with an increase in void fraction for M_SG1 and M_SG2, respectively. Natural circulation in two-phase should have a mass flow rate greater than the critical value for stable operation. Fig 14 shows the variation of CMFR with inlet void fraction for C_SG showing that the trend is not linear in this case. This is because of large length of the tube which increases the frictional forces non-monotonically. For void fraction greater than 0.3, the CMFR was always greater than the maximum safe operating flow rate limit set at void fraction 0.1. This leads to an unstable flow if the transients in void fraction go beyond 0.3 in C_SG.

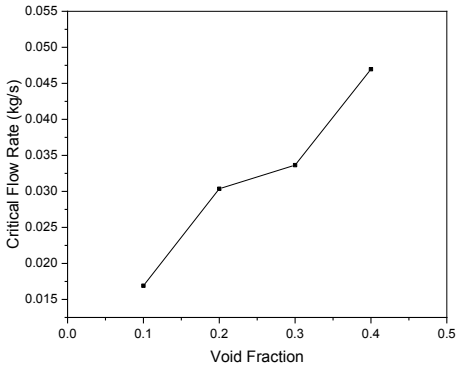

Fig 12. Variation of CMFR with inlet void fraction for M_SG1

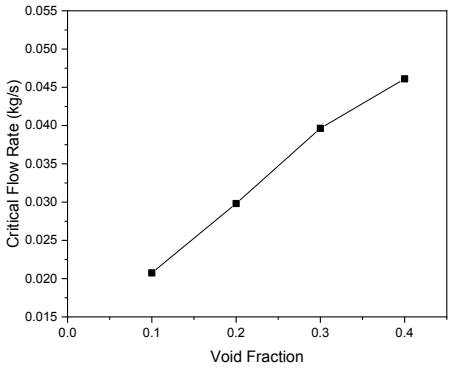

Fig 13. Variation of CMFR with inlet void fraction for M_SG2

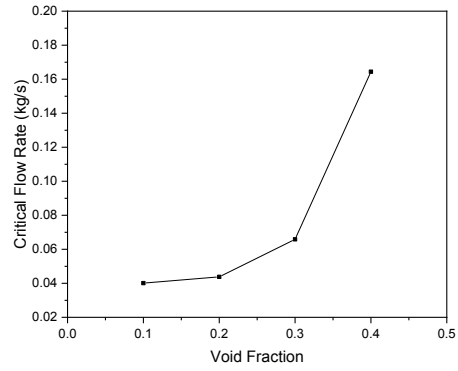

Fig 14. Variation of CMFR with inlet void fraction for M_SG2

6.4 Entrance Effect on Void Fraction Distribution along U-tube Length

The inclusion of the entrance effect (flow developing) for the U-tube greatly influences the distribution of void fraction with U-tube position as shown in Fig 15 and Fig 16 for M_SG1 and C_SG at CMFRs respectively. Because of the entrance effect, the void fraction initially increases in the hot leg and then started to decrease. This behavior is observed at all inlet void fractions and mass flow rates. It affects the C_SG at higher flow rates in a way to keep the characteristics curve in the unstable region.

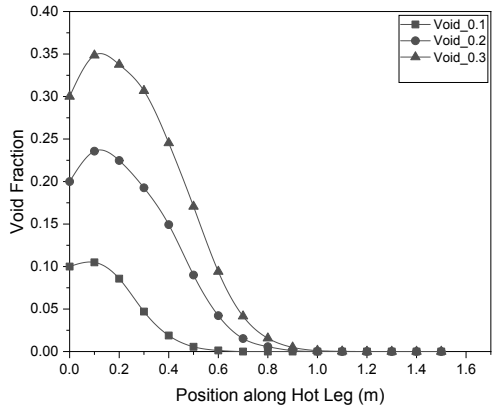

Fig 15. Void fraction distribution along U-tube hot leg for M_SG1

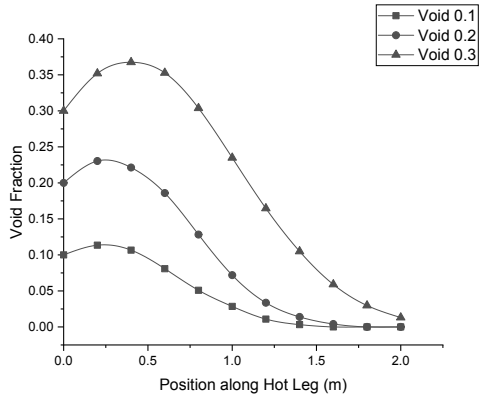

Fig 16. Void fraction distribution along U-tube hot leg for C_SG

7. Conclusion

The two-phase NC in U-tube SG is the key passive phenomenon to take out the reactor core heat in SBLOCA. But because of its non-linear nature, NC is susceptible to reverse flow, which greatly reduces the heat removal capability of SG and endangers the NPP operation. CFD method was used to study the inlet void fractions effects on CMFR in two marine NPP SG and one commercial SG. The effect of pipe roughness was also studied for one marine NPP SG. The main conclusions drawn were as follows:

1. The CMFR decreases with an increase in pipe roughness for the same flow conditions resulting in a wider stable region.
2. With an increase of inlet void fraction, the two-phase region increases at the same inlet slip ratio, inlet liquid velocity, and inlet gas velocity for all SGs.
3. An increase in inlet void fraction extends the unstable region at small inlet void fractions for small steam generators at which complete condensation occurs in the hot leg.
4. The CMFR increases with an increase in inlet void fraction for all SGs.
5. The minimum safe operating mass flow rate is dictated by the absolute maximum CMFR within the range of inlet void fraction transients.
6. The maximum safe operating mass flow rate is dictated by the point of transition from natural to forced circulation at a minimum void fraction in the range of transients.
7. The entrance effect changes the void fraction spatial distribution of the SGs in such a way that it increases to a certain maximum value greater than the inlet value and then started to increase.
8. The increase in void fraction due to entrance effects changes the characteristics curve and increases the unstable region in large SG.

References

[1] Z. Yang, J. Shan, J. J. N. E. Gou, and Design, "Preliminary assessment of a combined passive safety system for typical 3-loop PWR CPR1000," vol. 313, pp. 148-161, 2017.

[2] I. E. Agency and F. Birol, *World energy outlook*

2013. International Energy Agency Paris, 2013.

[3] K. Kawanishi, A. Tsuge, M. Fujiwara, T. Kohriyama, H. J. J. o. N. S. Nagumo, and Technology, "Experimental study on heat removal during cold leg small break LOCAs in PWRs," vol. 28, no. 6, pp. 555-569, 1991.

[4] V. Kouhia *et al.*, "Benchmark exercise on SBLOCA experiment of PWR PACTEL facility," vol. 59, pp. 149-156, 2013.

[5] S. Kim, W. J. N. E. Jang, and Technology, "The Simulation of Semicale Natural Circulation Test S-NC-3, S-NC-4 Using RELAP5/Mod3. 1," vol. 30, no. 5, pp. 424-434, 1998.

[6] Y. Kukita, H. Nakamura, K. Tasaka, C. J. N. S. Chauliac, and Engineering, "Nonuniform steam generator U-tube flow distribution during natural circulation tests in ROSA-IV large scale test facility," vol. 99, no. 4, pp. 289-298, 1988.

[7] B. Schoen, P. J. E. t. Weber, and f. science, "Nitrogen in a steam generator of a PWR under SBLOCA conditions: Experimental investigations in the PKL test facility and comparison with analytical studies," vol. 15, no. 3, pp. 238-252, 1997.

[8] Y.-M. Ferng, C.-H. J. N. e. Lee, and design, "Numerical simulation of natural circulation experiments conducted at the IIST facility," vol. 148, no. 1, pp. 119-128, 1994.

[9] Y.-J. Chung, H.-C. Kim, and M.-H. J. J.-K. N. S. Chang, "Post test analysis to natural circulation experiment on the BETHSY facility using the MARS 1.4 code," vol. 33, no. 6, pp. 638-651, 2001.

[10] J. Sanders, "Stability of single-phase natural circulation with inverted U-tube steam generators," 1988.

[11] J. Hao, W. Chen, and D. Zhang, "Effect of U-tube length on reverse flow in UTSG primary side under natural circulation," *Annals of Nuclear Energy,* vol. 56, pp. 66-70, 2013.

[12] J. Hao, W. Chen, and S. J. P. i. N. E. Wang, "Flow instability analysis of U-tubes in SG based on CFD method," vol. 70, pp. 134-139, 2014.

[13] J. Hao, W. Chen, G. Hu, X. Chu, D. Zhang, and L. Yu, "Experimental research on reverse flow critical point among parallel U-tubes in SG," *Progress in Nuclear Energy,* vol. 98, pp. 59-70, 2017.

[14] B. Yang, C. Wang, and X.-J. J. A. o. N. E. Li, "Analysis of single phase flow instability in U-tubes of steam generator," vol. 109, pp. 180-184, 2017.

[15] J.-J. Jeong, M. Hwang, Y. J. Lee, and B. D. Chung, "Non-uniform flow distribution in the steam generator U-tubes of a pressurized water reactor plant during single- and two-phase natural circulations," *Nuclear Engineering and Design,* vol. 231, no. 3, pp. 303-314, 2004.

[16] G. Hu, L. Yu, W. Chen, J. Hao, and X. J. P. i. N. E. Chu, "Experimental and numerical investigations on the reverse flow phenomena in UTSGs," vol. 92, pp. 147-154, 2016.

[17] M. Shen *et al.*, "Investigation on reverse flow phenomenon in UTSGs with abnormal secondary side water level under single-phase natural circulation," *Progress in Nuclear Energy,* vol. 119, 2020.

[18] X. Chu, M. Li, W. Chen, and J. Hao, "Investigation on reverse flow characteristics in U-tubes under two-phase natural circulation," *Nuclear Engineering and Technology,* vol. 52, no. 5, pp. 889-896, 2020.

[19] X. Chu, W. Chen, Y. Shang, J. Hao, and D. Zhang, "CFD investigation on reverse flow characteristics in U-tubes under two-phase natural circulation," *Progress in Nuclear Energy,* vol. 114, pp. 145-154, 2019.

[20] P. Ansys Inc %J Canonsburg, Release 15.0, "ANSYS FLUENT theory guide," ed: Cannonsburg, PA, USA: ANSYS, Inc, 2013.

[21] D. Sun, J. Xu, and Q. J. N. H. T. Chen, Part B: Fundamentals, "Modeling of the evaporation and condensation phase-change problems with FLUENT," vol. 66, no. 4, pp. 326-342, 2014.

[22] K. C. Jain, "Self-sustained hydrodynamic oscillations in a natural-circulation two-phase-flow boiling loop," Argonne National Lab., Ill.1965.

[23] A. K. Nayak and P. K. Vijayan, "Flow Instabilities in Boiling Two-Phase Natural Circulation Systems: A Review," *Science and Technology of Nuclear Installations,* vol. 2008, pp. 1-15, 2008.